Aerospace Science and Technology 61 (2017) 11–20

Contents lists available at ScienceDirect

Aerospace Science and Technology

www.elsevier.com/locate/aescte

Lévy flight based pigeon-inspired optimization for control parameters optimization in automatic carrier landing system

Rui Dou, Haibin Duan *

State Key Laboratory of Virtual Reality Technology and Systems, School of Automation Science and Electrical Engineering, Beihang University (formerly Beijing University of Aeronautics and Astronautics, BUAA), Beijing 100191, PR China

ARTICLE INFO

Article history:
Received 6 July 2016
Received in revised form 13 October 2016
Accepted 15 November 2016
Available online 18 November 2016

Keywords:
Carrier landing
Automatic carrier landing system (ACLS)
Pigeon inspired optimization (PIO)
Lévy flight

ABSTRACT

In this paper, we conduct the design of the automatic carrier landing system (ACLS) for aircraft, which can integrates the aircraft flight control system, throttle control system, inertial navigation sensors, and shipboard AN/SPN-42 tracking radar and computer system to achieve fully automatic approach control to the carrier deck in all weather conditions. In order to obtain the better dynamic response of the longitude command, a novel control parameter design method is presented for the automatic carrier landing system. To overcome difficulties in the manual parameter adjustment task, the Lévy flight based pigeon-inspired optimization (PIO) algorithm is utilized by converting the parameter design problem to an optimization problem. To optimize control parameters in the H-Dot autopilot and the approach power compensation system, a weighted linear cost function in the time domain is adopted. Series of experiments are conducted to demonstrate the feasibility and effectiveness of our method. Comparative results indicate that our method is much better than other methods. With the help of the optimization algorithm, ACLS can have better performance in dynamic responses.

1. Introduction

Landing aircrafts on the carrier can be a daunting task due to the ship motion and the air turbulence, which requires precise control of the flight path within the narrow landing window. To help ease pilot's assignment, automatic carrier landing system (ACLS) has been developed. In general, ACLS consists of the carrier tracking radar, radio data link, control systems and digital computers. It provides automatic control of the flight path angle and approaching speed. After the measurement of aircraft motion, control command is calculated and sent to the aircraft to achieve accurate flight path control.

Aircraft flight control system designed for these requirements is made up of the aircraft autopilot and the approach power compensation system (APC), so that it can provide automatic flight and thrust control [1]. According to the process of automatic landing, the ship borne radar system to track the position of the aircraft and calculate the H-Dot command [2–4]. After that, the command is transmitted to the aircraft via a data link. Flight control system H-Dot command to control the aircraft slid along the precise flight path while the approach power compensation system keep the angle of attack at a constant value [5].

The ACLS' design goal is to achieve a precise landing in low visibility weather, night visibility conditions, with the deck motion due to the high seas and the air behind the carrier, which calls for a very high demand towards the choice of the parameters in the ACLS. It's a very difficult and time-consuming task for the designer to adjust the parameters so as to achieve the rapid and accurate response to the command signal, especially when the control system has the coupled control structure with a large number of parameters.

Parameter adjusting by intelligent optimization algorithm is a very effective and practical way to acquire the optimal parameters for the control system, which gains more and more popularity in recent years. Lots of population-based swarm intelligence algorithms were put forward, such as ant colony optimization (ACO) [6], particle swarm optimization (PSO) [7], artificial bee colony (ABC) algorithm [8,9], differential evolution (DE) algorithm [10], brain storm optimization (BSO) [11–14] and so on. Many researchers have applied these bio-inspired optimization algorithms to the parameters optimization problem and achieved remarkable success in their studies.

In recent years, many new bio-inspired optimization algorithms were proposed. All these algorithms were trying to offer the optimization problems with better practical solution. Among them, a

* Corresponding author.
E-mail address: hbduan@buaa.edu.cn (H. Duan).

http://dx.doi.org/10.1016/j.ast.2016.11.012
1270-9638/

new bio-inspired optimization algorithm, namely pigeon-inspired optimization (PIO) algorithm, which was firstly proposed by Duan and Qiao [15] in 2014, is a method that cannot be underestimated. According to the behavior of pigeons in finding the destination, the algorithm consists of two operators. Map and compass operator is based on magnetic field and sun, while the landmark operator is based on the landmark. The feasibility and the rapidness of the algorithm have already been proved by many researchers, and they applied this algorithm to solve several optimization problems and made PIO more effective [16–23].

In this study, we make some improvement to the basic PIO by redesigning the two operators with Lévy flight walk model [24,25], and name the new algorithm Lévy flight based pigeon-inspired optimization (LFPIO). To illustrate the effectiveness of LFPIO, we apply LFPIO, PIO, PSO and DE to optimize the control parameters in the F/A-18A ACLS. The control parameters in the H-Dot command autopilot and APCS are optimized by minimizing the cost functions defined in the time domain.

The remainder of this paper is organized as follows. In Section 2, we briefly introduce the 6-DOF (six-degree-of-freedom) nonlinear dynamic model of F/A-18A, and descriptions of the main components of ACLS including the inner loop, the H-Dot autopilot loop and APCS in this section. A detailed introduction of the basic PIO and the detail of LFPIO algorithm will be introduced in Section 3. In Section 4, the control parameter optimization method based on LFPIO and the cost function are presented, followed by comparative experimental simulation and result analysis in Section 5. Finally, our concluding remarks are given in the last section.

2. Automatic carrier landing system

2.1. Longitude dynamic model of unmanned aerial vehicle

In this work, a 6-DOF motion model was considered. Supposing ground coordinate system for the inertial coordinate system, unmanned aerial vehicles to be rigid and its mass and center of gravity does not change over time.

According to the theory of 6-DOF motion of a rigid body, aircraft navigation space equations are:

$$\begin{Bmatrix}\dot{x}\\ \dot{y}\\ \dot{z}\end{Bmatrix}=\begin{bmatrix}\cos\theta\cos\psi & \sin\theta\cos\psi\sin\phi-\sin\psi\cos\phi & \sin\theta\cos\psi\cos\phi+\sin\psi\sin\phi\\ \cos\theta\sin\psi & \sin\theta\sin\psi\sin\phi+\cos\psi\cos\phi & \sin\theta\sin\psi\cos\phi-\cos\psi\sin\phi\\ -\sin\theta & \cos\theta\sin\phi & \cos\theta\cos\phi\end{bmatrix}\begin{Bmatrix}u\\ v\\ w\end{Bmatrix} \tag{1}$$

Equations of motion for the aircraft are as following:

$$\begin{Bmatrix}\dot{\phi}\\ \dot{\theta}\\ \dot{\psi}\end{Bmatrix}=\begin{bmatrix}1 & \sin\phi\tan\theta & \cos\phi\tan\theta\\ 0 & \cos\phi & -\sin\phi\\ 0 & \sin\phi\sec\theta & \cos\phi\sec\theta\end{bmatrix}\begin{Bmatrix}p\\ q\\ r\end{Bmatrix} \tag{2}$$

Three other forces except for the gravity in the body axis component are as following:

$$\begin{Bmatrix}\dot{u}\\ \dot{v}\\ \dot{w}\end{Bmatrix}=g\begin{Bmatrix}-\sin\theta\\ \sin\phi\cos\theta\\ \cos\phi\cos\theta\end{Bmatrix}+\begin{bmatrix}0 & r & -q\\ -r & 0 & p\\ q & -p & 0\end{bmatrix}\begin{Bmatrix}u\\ v\\ w\end{Bmatrix}+\frac{1}{m}\begin{Bmatrix}F_x\\ F_y\\ F_z\end{Bmatrix} \tag{3}$$

The force equations are as following:

$$\begin{Bmatrix}\dot{u}\\ \dot{v}\\ \dot{w}\end{Bmatrix}=g\begin{Bmatrix}-\sin\theta\\ \sin\phi\cos\theta\\ \cos\phi\cos\theta\end{Bmatrix}+\begin{bmatrix}0 & r & -q\\ -r & 0 & p\\ q & -p & 0\end{bmatrix}\begin{Bmatrix}u\\ v\\ w\end{Bmatrix}+\frac{1}{m}\begin{Bmatrix}F_x\\ F_y\\ F_z\end{Bmatrix} \tag{4}$$

The moment equations are as following:

$$\begin{Bmatrix}\dot{p}\\ \dot{q}\\ \dot{r}\end{Bmatrix}=\begin{bmatrix}(c_1r+c_2p)q\\ c_5pr-c_6(p^2-r^2)\\ (c_8p-c_2r)q\end{bmatrix}+\begin{bmatrix}c_3\bar{L}+c_4N\\ c_7M\\ c_4\bar{L}+c_9N\end{bmatrix} \tag{5}$$

where $c_1, c_2, \ldots$ and c_9 in Eq. (5) stand for the constant of inertia respectively as follows.

$$c_1=\frac{(I_y-I_z)I_z-I_{xz}^2}{\Sigma},\quad c_2=\frac{(I_x-I_y+I_z)I_{xz}}{\Sigma},\quad c_3=\frac{I_z}{\Sigma},$$
$$c_4=\frac{I_{xz}}{\Sigma},\quad c_5=\frac{I_z-I_x}{I_y},\quad c_6=\frac{I_{xz}}{I_y},\quad c_7=\frac{1}{I_y},$$
$$c_8=\frac{I_x(I_x-I_y)+I_{xz}^2}{\Sigma},\quad c_9=\frac{I_x}{\Sigma},\quad \Sigma=I_xI_z-I_{xz}^2$$

Considering the aircraft model with conventional control surfaces, the aerodynamic forces and moments in the model can be obtained by the calculation of the aerodynamic derivatives as follows:

$$\begin{Bmatrix}D\\ Y\\ L\end{Bmatrix}=\frac{1}{2}\rho V^2S\begin{Bmatrix}C_{D0}+C_{D\alpha}\alpha\\ C_{Y\beta}\beta\\ C_{L0}+C_{L\alpha}\alpha+C_{L\delta_e}\delta_e\end{Bmatrix} \tag{6}$$

$$\begin{Bmatrix}\bar{L}\\ M\\ N\end{Bmatrix}=\frac{1}{2}\rho V^2S\begin{Bmatrix}b(C_{l\beta}\beta+C_{lp}\cdot b/2V\cdot p+C_{lr}\cdot b/2V\cdot r+C_{l\delta_a}\delta_a+C_{l\delta_r}\delta_r)\\ c(C_{m0}+C_{m\alpha}\alpha+C_{mq}\cdot c/2V\cdot q+C_{m\delta_e}\delta_e)\\ b(C_{n\beta}\beta+C_{lp}\cdot b/2V\cdot p+C_{lr}\cdot b/2V\cdot r+C_{n\delta_a}\delta_a+C_{n\delta_r}\delta_r)\end{Bmatrix} \tag{7}$$

where (x, y, z) are the variation of position, (p, q, r) are the angular velocity of the body around axis of rotation, (u, v, w) along the body axis motion linear velocity, (ϕ, θ, ψ) are roll angle, pitch and yaw angles, $(\bar{L}, M, N)$ are rolling moment, pitching moment and yawing moment, (D, Y, L) are the drag force, the lateral force and the lift. δ_e, δ_a and δ_r are the deflection of elevator, the aileron and the rudder.

2.2. Vertical rate referenced autopilot

Based on the aircraft model, the ACLS is designed to be consist of three parts: the inner loop, the APCS and the H-Dot autopilot [1,5]. In fact, the controller for the ACLS in this paper is similar to the traditional PID controller. The autopilot and approach power compensation system use these attitude angle commands to control the flight-path angle of the aircraft to eliminate the altitude error.

In the control structure of the inner loop as shown in Fig. 1, the pitch rate is controlled to achieve rapid dynamic response. A structure filter and a lag-lead filter are utilized in the feedback loop in order to reduce the noise in high frequency and avoid the body structure resonance of the plane.

Generally, as the speed of aircraft almost remain unchanged during the carrier landing, the vertical rate can be described as $\dot{h}=V\sin\gamma$, where V is the velocity and γ is the flight path angle. To maintain the aircraft tracing a landing path, the control of the

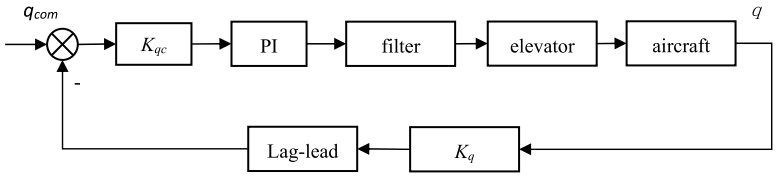

Fig. 1. Block diagram of ACLS inner loop.

path angle can be converted to the control of the vertical rate [2]. Thus, the H-Dot command autopilot utilizes the vertical rate signal as the feedback signal. To increase the damping ratio, the vertical accelerate signal is introduced in the feedback loop.

As the control of the vertical rate is equivalent to the control of the flight path angle, and the differential of the vertical rate can be proportional to normal overload. Thus we can use the flight path angle and the normal overload as feedback to the vertical rate autopilot so as to reduce the noise caused by direct differential.

2.3. APCS with constant angle of attack

The autopilot response to the commanded pitch angle, but the flight-path angle must be controlled as well in the automatic landing system by keeping the angle of attack of the airplane. To ensure the aircraft tracing a landing path with the constant angle of attack and velocity, the APCS is applied. The commonly used approach power compensation system includes the structure of keeping constant speed and constant angle of attack. Previous researches have done lots of research to demonstrate that the path angle can track the pitch angle quickly and accurately under the control of the approach power compensation system with constant angle of attack [1]. So we design an approach power compensation system with the structure of keeping constant angle of attack in this paper.

In this paper, four signals are adopted in the APCS as the feedback signals, namely the angle of attack, the normal overload, the pitch rate and the elevator command. The angle of attack is designed to trace a constant command angle. The normal overload was designed to increase the speed of response. The pitch rate signal can increase the damping ratio. The elevator command signal can relieve the deflection of the elevator.

3. Lévy flight based PIO optimized algorithm

3.1. The basic PIO algorithm

PIO algorithm is a new kind of particle swarm optimization method from pigeon's behavior, which requires personal and global optimization and local optimal information particle. PIO is made up of two operators according to the behavior of pigeons in finding the destination. They are map and compass operator and landmark operator, with the help of the individual and global best position in conduction of the two operators, they achieve better performance in searching destination.

(1) Map and compass operator:

In this operator, the rules are defined with the position X_i and the velocity V_i of pigeon i, and the position and velocity in a D-dimension search space are updated in each iteration. The new position and velocity of pigeon i at the t-th iteration can be calculated with the following equations:

$$V_i(t) = V_i(t-1) \cdot e^{-Rt} + \text{rand} \cdot \left(X_g - X_i(t-1)\right) \tag{8}$$

$$X_i(t) = X_i(t-1) + V_i(t) \tag{9}$$

where R is the map and compass factor, *rand* is a random number ranging from 0 to 1, and X_g is the current global best position, which can be obtained by comparing all the positions of the pigeons.

(2) Landmark operator:

In this operator, half of the number of the pigeons are decreased in every generation. In order to get to the destination quickly, the rest of the pigeons fly straight to the destination. Let the X_c be the center position of the pigeons, the position updating rule for pigeon i at the t-th iteration are given in the following equations:

$$N_p(t) = \frac{N_p(t-1)}{2} \tag{10}$$

$$X_c(t) = \frac{\sum X_i(t) \cdot \text{fitness}(X_i(t))}{N_p \cdot \sum \text{fitness}(X_i(t))} \tag{11}$$

$$X_i(t) = X_i(t-1) + \text{rand} \cdot \left(X_c(t) - X_i(t-1)\right) \tag{12}$$

where N_p is the number of the pigeons, while the fitness is the cost function of a pigeon. For minimum optimization, we can choose the minimum to be the destination function.

3.2. Lévy flight based PIO algorithm

To improve the PIO algorithm, we redesigned two operators instead of basic operators. Two new operators, namely Lévy flight based map and compass operator and *logsig* function based landmark operator, are given as follows:

(1) Map and Compass operator with Lévy flight walk model

Lévy flight has been demonstrated that it is the best one of random walk models and is a Markov process [29]. In the process of walking, the step length is a heavy-tailed Lévy distribution. The simplified Lévy flight can be described as following:

$$L(s) \sim |s|^{-1-\delta} \tag{13}$$

where s denotes random step length and $0 < \delta \leq 2$ is an index. When searching a unknown and large-scale space, Lévy flight is more effective than Brown motion, because the variance of Lévy flight increases more rapidly. The two kinds of variances are shown as follows:

$$\sigma^2_{Brown}(s) \sim s \tag{14}$$

$$\sigma^2_{Levy}(s) \sim s^{3-\delta}, \quad 1 < \delta \leq 2 \tag{15}$$

In Lévy flight, some solutions execute local search, and others execute global search. This mechanism can balance the diversity and the convergence speed. At the same time, Lévy flight can simulate the search behaviors of some animals such as the fish school, the pigeon flock and the wolf pack. Hence, we use this mechanism to design the new map and compass operator. Here, Lévy flight can be implemented by Mantegna's algorithm [30], and the operator can be implemented by following equations:

$$X_t = X_p(t-1) + step \circ \boldsymbol{randn} \tag{16}$$

$$step = s \oplus \left(X(t-1) - X_g\right) \tag{17}$$

$$s = \frac{\mu}{|v|^{1/\delta}}, \quad \delta = 1.5 \tag{18}$$

$$\mu \sim N(0, \sigma_\mu^2), \quad v \sim N(0, \sigma_v^2) \tag{19}$$

$$\sigma_\mu = \left\{ \frac{\Gamma(1+\delta)\sin(\pi\delta/2)}{\Gamma[(1+\delta)/2]\delta \cdot 2^{(\delta-1)/2}} \right\}^{1/\delta}, \quad \sigma_v = 1 \tag{20}$$

where N denotes the normal distribution, s represent random step length and X are vectors, $\oplus$ denotes the Hadamard product, and ***randn*** is also a vector in which each element is a random number obeyed normal distribution. In addition, the elite selection strategy is utilized to improve the ability of local search and described by the following equation:

$$\begin{cases} X_p(t) = X_t, & \text{if } fitness(X_t) < fitness(X_p(t-1)) \\ X_p(t) = X_p(t-1), & \text{if } fitness(X_t) \geq fitness(X_p(t-1)) \end{cases} \tag{21}$$

(2) Landmark operator with logsig function

In PIO algorithm, the landmark operator can accelerate the convergence of algorithm. However, the operator easily leads to the premature convergence, and all solution will be trapped into local optima. In order to avoid the problem, we adopt the adaptive logsig function [12] to adjust the step length of search. Detailed equations are given as follows:

$$X_t^j = X_p^j(t-1) + Length \cdot \boldsymbol{randn} \oplus \left(X_g - X^j(t-1)\right) \tag{22}$$

$$Length = \text{logsig}\left(\frac{Nc \cdot \zeta - I}{k}\right) \tag{23}$$

where j denotes the j-th dimension of solution, ζ and k are the adaptive parameters of *logsig* function. The parameter ζ decides when the search converges.

4. Control parameters optimization based on LFPIO

4.1. Problem formation

The control gains tuning of the vertical rate referenced guidance system and the approach power compensation system can be treated as the typical continual spatial optimization problem.

Our purpose is that the ACLS can remain the angle of attack while the vertical rate autopilot can response in an accuracy and fast way. Here we choose six control parameters to be optimized from the h-dot autopilot and APCS as shown in Fig. 2 and Fig. 3:

$$X = [K_1, K_2, K_3, K_4, K_5, K_6]$$

As the control system in APCS and h-dot autopilot are coupled each other, it's necessary to achieve the optimization of both systems at the same time. According to the function of both systems, we need to eliminate the error between the angle of attack and the reference command while keeping the vertical rate response in a rapid and accurate way. Hence, we put forward the cost function of this multi-object optimization problem as follows.

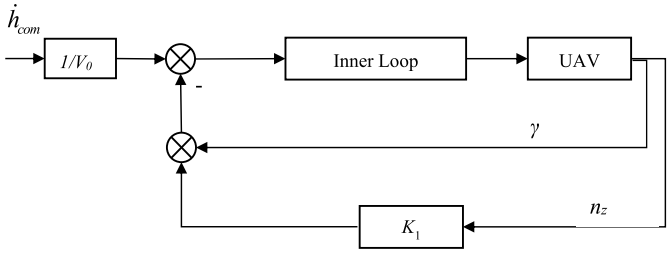

Fig. 2. Block diagram of ACLS outer loop.

The first cost function aims to eliminate the error between the attack angle and the reference attack angle command. We achieved this purpose by calculating the integration of the absolute value of the error which is defined as following:

$$f_1 = \int |\alpha(t) - \alpha_{com}| dt \tag{24}$$

The second cost function represents the requirement of keeping a good response of the vertical rate. We transfer this problem into one which can reduce the error between the vertical rate and the vertical rate command as following:

$$f_2 = \int |\dot{h}(t) - \dot{h}_{com}| dt \tag{25}$$

As the control parameter optimization is a multi-objective optimization problem. In this paper, we use the weighting method to solve this problem. The two objective functions defined above are combined into one cost function using different weighting factors:

$$f = \omega_1 f_1 + \omega_2 f_2 \tag{26}$$

where ω_1 and ω_2 are the weighting factors of the two fitness functions.

4.2. Implementation procedure of LFPIO for parameter optimization

The procedure of ACLS parameter optimization based on the LFPIO algorithm is as following:

Step 1: Initialize the parameters in LFPIO algorithm, namely the space dimension D, the population size N_p, the maximum iteration number $Nc_{\max}$ and the control parameter k in logsig function and initial the random set of the pigeons.

Step 2: Evaluate the fitness function of pigeons. The parameters of each individual are initialized in Step 1. Subsequently, utilize the Eq. (26) to compute the fitness value of the pigeons.

Step 3: Conduct the Lévy flight operator to generate new pigeon according to Eq. (16) and Eq. (17).

Step 4: Update the elite individual according to Eq. (21).

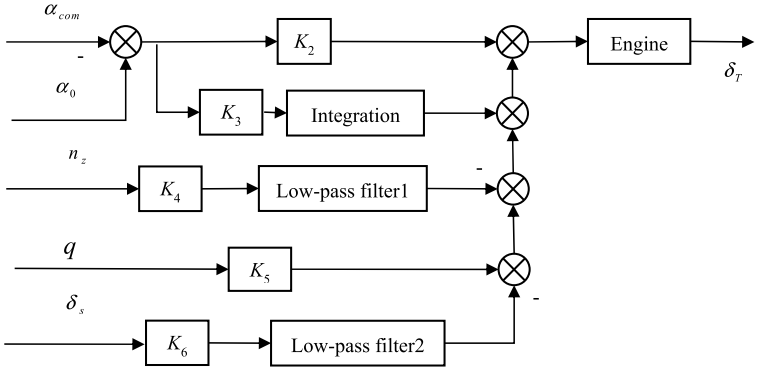

Fig. 3. Block diagram of APCS.

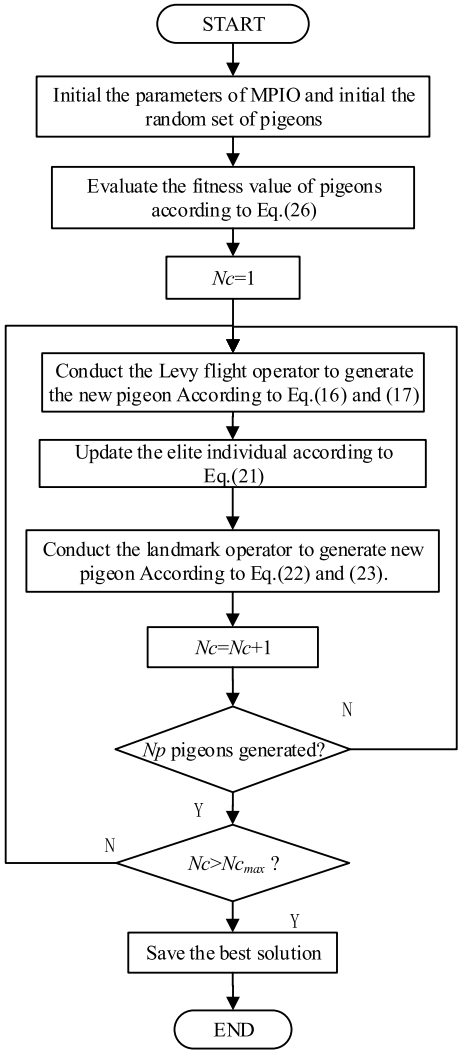

Fig. 4. Flow chart of the LFPIO algorithm for ACLS parameter optimization.

Step 5: According to Eqs. (22) and (23), conduct the landmark operator to generate new pigeon.

Step 6: If N_p pigeons have been generated, go to Step 7. Otherwise, go to Step 3.

Table 1
Geometric parameters of aircraft.

Mass m (kg)	Geometric mean chord c (m)	Span b (m)	Wing area S (m^2)
14000	3.488	11.4	37.16
I_x ($kg\,m^2$)	I_y ($kg\,m^2$)	I_z ($kg\,m^2$)	I_{xz} ($kg\,m^2$)
31184	156910	230411	−4028

Step 7: Output the results when the current number of iterations Nc reaches $Nc_{\max}$. Otherwise, go to Step 3.

The flow chart of the proposed LFPIO for ACLS parameters optimization problem is shown in Fig. 4.

5. Simulation and analysis

In order to demonstrate the effectiveness of the LPIO algorithm, comparative experiments of LFPIO algorithm with other algorithms in the optimization of ACLS parameters were conducted. All experiments are performed using MATLAB R2014b on a PC with a Core II 2.4 GHz CPU and 4 G of RAM. The response of the angle of attack and the vertical rate were compared and analyzed. The experiment of the aircraft landing through the wind disturbance was also conducted.

5.1. Simulink block of ACLS

In this paper, F/A-18A geometric parameters and aerodynamic derivatives [26–28] were used to set up the longitude dynamic model of the aircraft as shown in Tables 1 and 2.

As the landing process of the craft in on al low height above the sea, we choice the sea level height as the trim height. The trim values of the longitude states are: $V_0 = 69.96$ m/s, $\gamma_0 = -3.5$ deg and $\alpha_0 = 8.1$ deg.

The inner loop of autopilot of the unmanned aerial vehicle Simulink block was set up as shown in Fig. 5 below, considering the limitation of the elevator, the amplitude limit is from −24° to 10.5° and the speed limit is from −40° to 40°.

The frequency response between the ACLS inner loop with lag-lead filter and the common CAS with unit negative feedback comparison is shown as following in Fig. 6.

The inner loop structure with the feedback structure has a large gain in the middle and low frequency segment, and it can effectively improve the dynamic characteristics of the system compared to the conventional structure in the phase.

Table 2
Aerodynamic derivatives of aircraft.

Drag coefficient, lateral force coefficient, lift coefficient	C_{D0}	$C_{D\alpha}$	$C_{Y\beta}$	C_{L0}	$C_{L\alpha}$	$C_{L\delta_e}$
	0.1027	0.7476	−0.8022	0.8229	2.7584	0.4894
Rolling moment coefficient	$C_{l\beta}$	C_{lp}	C_{lr}	$C_{l\delta_a}$	$C_{l\delta_r}$	
	−0.1203	−0.38	0.013	0.1834	0.0172	
Pitching moment coefficient	C_{m0}	$C_{m\alpha}$	C_{mq}	$C_{m\delta_e}$		
	0.0603	−0.4260	−3.5432	−0.6596		
Yawing moment coefficient	$C_{n\beta}$	C_{np}	C_{nr}	$C_{n\delta_a}$	$C_{n\delta_r}$	
	0.0974	−0.0503	−0.2401	0.0115	−0.0859	

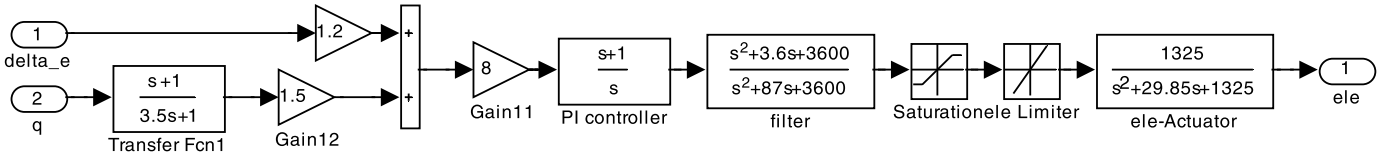

Fig. 5. Simulink block of inner loop.

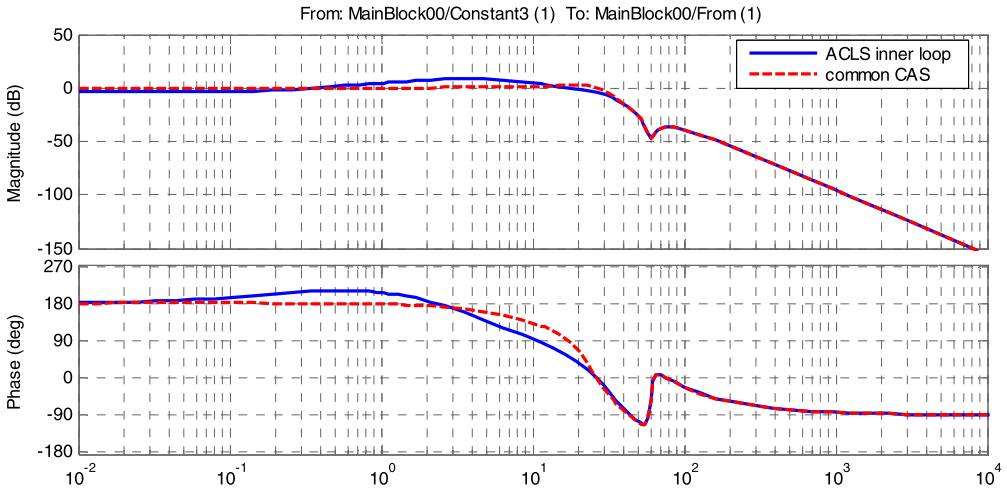

Fig. 6. Frequency response comparison.

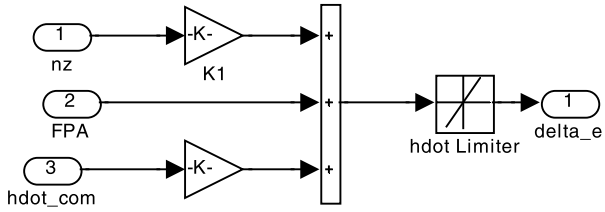

Fig. 7. Simulink block of H-Dot autopilot loop.

Based on the structure of the inner loop of the autopilot, the flight path angle and the normal overload were used as feedback to the vertical rate control and the angle of attack, the normal overload, the pitch rate and the elevator command were used as the feedback signal for APCS. The Simulink block was built as shown in Fig. 7 and Fig. 8.

Based on the structure of autopilot and APCS, a PID-type guidance system was built to guide the aircraft to land on the carrier while tracing the expected H-Dot command. The Simulink block is shown in Fig. 9.

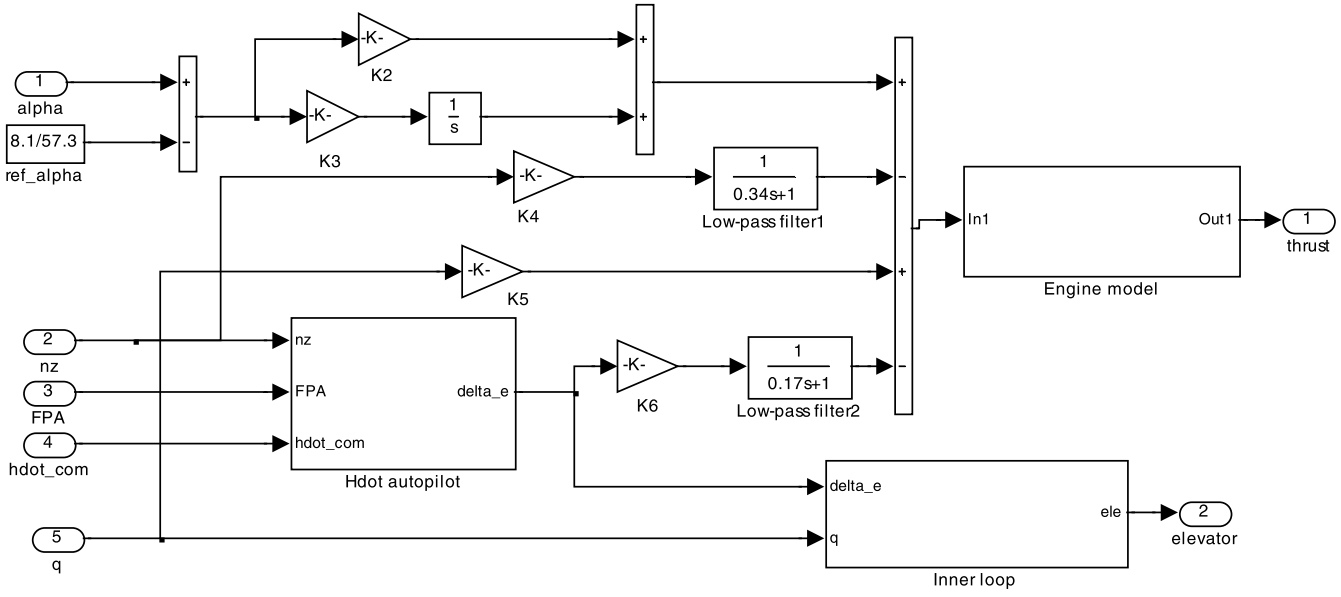

Fig. 8. Simulink block of APCS.

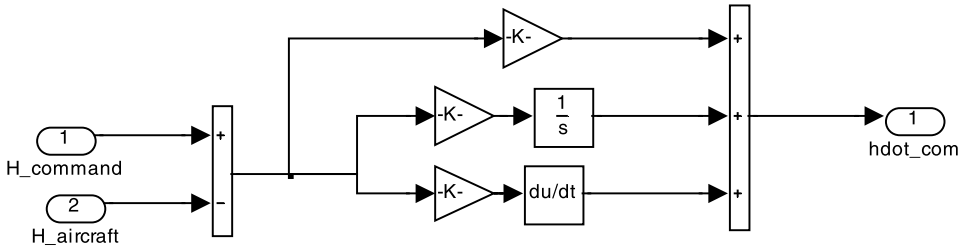

Fig. 9. Simulink block of guidance system.

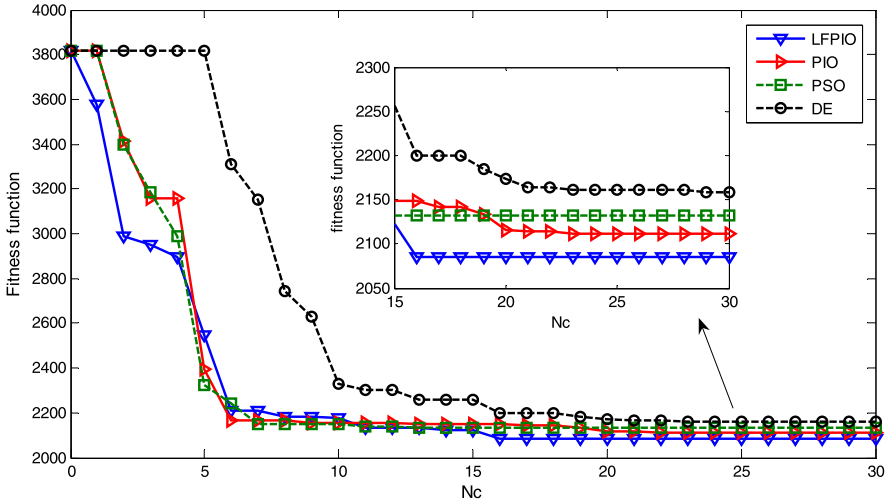

Fig. 10. Comparative cost function of LFPIO with other optimizations.

Table 3
Comparative optimization results.

Algorithm	Control parameters						Fitness value
	K_1	K_2	K_3	K_4	K_5	K_6	
LFPIO	0.01	1.9886	0.0393	1.4172	0.0684	1.4458	2085.88
PIO	0.01	3.00	0.01	1.7131	0.3590	0.01	2111
PSO	0.01	3.00	0.01	1.7561	0.01	0.5712	2132.7
DE	0.0162	2.1322	0.0127	1.6739	0.9499	0.1571	2158.9

5.2. Optimization results of ACLS

Due to the fast convergence speed and the ability to jump out of the local optimum, many classical optimization algorithm were adopted to the field of the control parameter optimization, such as differential evolution (DE) algorithm and the particle swarm optimization (PSO). DE optimizes a problem by maintaining a population of candidate solutions and creating new candidate solutions by combining existing ones according to its simple formulae, and then keeping whichever candidate solution has the best score or fitness on the optimization problem at hand. PSO solves a problem by having a population of candidate solutions, here dubbed particles, and moving these particles around in the search-space according to simple mathematical formulae over the particle's position and velocity. They can optimize a problem by iteratively trying to improve a candidate solution with regard to a given measure of quality. In order to investigate the feasibility and effectiveness of the Lévy flight based PIO (LFPIO) algorithm with Lévy flight approach for adjusting of automatic landing system parameters, the comparative experiments with DE, PSO, the original PIO was conducted.

To ensure fair and valid comparisons, initialization parts of these optimization methods are the same, which can avoid the effect of initialization. Parameters such as the population size and the maximum iteration number are also consistent. The population size and the iteration number are both set to be 30. Search range of the parameters ranging from 0.01 to 3. Comparative fitness function results are shown in Fig. 10.

The final optimization results generated by LFPIO, PIO, PSO and DE algorithms and the minimum fitness function values are shown in the Table 3 respectively.

From Fig. 10 and Table 3, it's easy to find that starting from the same initial fitness function value, LFPIO can attain the lowest fitness function value among these optimization algorithms. The final fitness function value of basic PIO is higher than that of LFPIO, which demonstrates the improvement with the help of Lévy flight walk model and new logsig function. Although, basic PIO and PSO algorithm can also converge very quickly during the first 10 iterations as shown in the curve above, they fall into the local optimal solution at about 20 iterations while LFPIO can keep on searching to reach a lower fitness function value. As a conclusion, LFPIO algorithm has a faster convergence speed and better optimization ability than other algorithms do.

In order to verify the effectiveness of the optimization, series of experiments were conducted to present the comparative results of the responses of angle of attack and vertical rate as follows.

Suppose the AIRCRAFT fly in the steady level flight state initially, given the AIRCRAFT 5 m/s $\dot{h}_{com}$ command and the reference angle of attack command of 8.1°, the comparative response of the angle of attack, the vertical rate, the pitch angle and the pitch rate are illustrated respectively as follows.

It's obvious that from the curves of comparative experiments in Fig. 11, ACLS with APCS can eliminate the error of angle of attack with the parameters optimized by algorithms in this paper with different dynamic response. DE optimized ACLS with the highest fitness function value has greater negative overshoot than the rest in the error of angle of attack. Though response from PSO has the smallest negative overshoot, it takes much longer time to eliminate the error than the rest. LFPIO optimized control system has a faster response and less oscillation in angle of attack compared with the rest.

From the curves of comparative experiments in Fig. 12, vertical rate autopilot can also eliminate the error of vertical rate with the parameters optimized by algorithms in this paper. DE optimized ACLS has an overshoot at about 20% in the response of vertical rate while the rest are no more than 12%. ACLS optimized by LFPIO and PIO can eliminate the error and only need adjustment time of 5 s to while ACLS optimized by PSO requires 5.5 s.

LFPIO and PIO optimized ACLS take about 6 s to reach the steady in the pitch angle response as shown in Fig. 13 while PSO and DE optimized ACLS have the adjustment time for about 8 s.

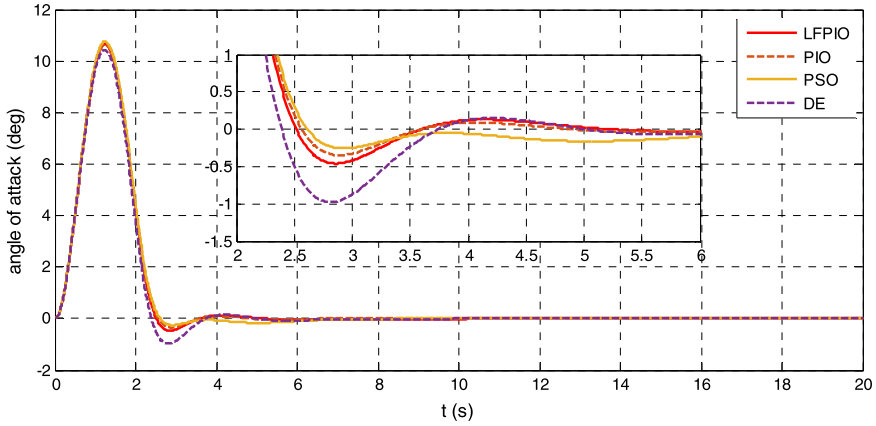

Fig. 11. Comparative results of error of angle of attack.

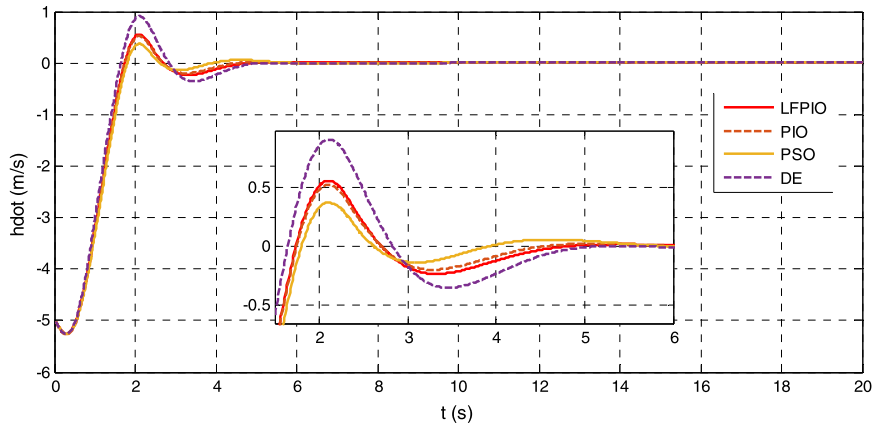

Fig. 12. Comparative results of error of h-dot.

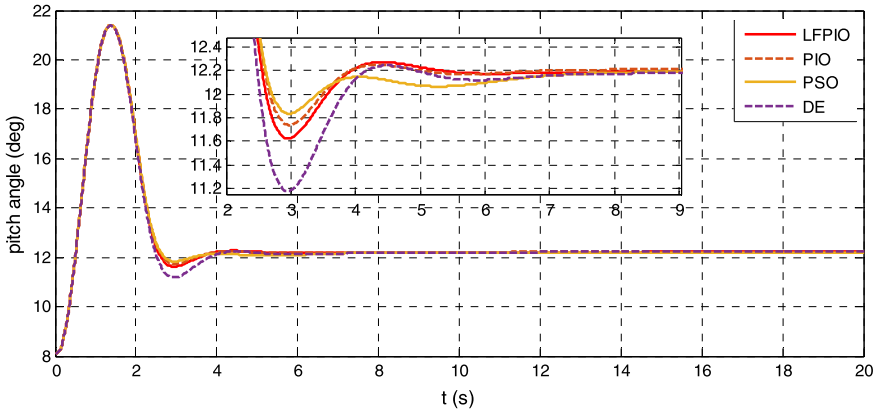

Fig. 13. Comparative results of pitch angle.

LFPIO optimized ACLS can also have more steady performance in pitch rate response as shown in Fig. 14.

It can be concluded that aircraft had better dynamic response by using the control parameters generated by LFPIO, which means it can acquire more stability and rapidity with the help of LFPIO algorithm.

Based on the LFPIO optimized control parameters, given the AIRCRAFT slop altitude command through the vertical wind disturbance of −4 to 4 m/s. The results of the vertical wind disturbance is shown in Fig. 15, while the altitude command and the response of the aircraft is shown in Fig. 16, and the error of the altitude response is given in Fig. 17.

From the landing experiments results in Figs. 16 and 17, the aircraft can accurately track the altitude command in about 20 s and the maximum altitude error is less than 12 m. The vertical wind disturbance doesn't have significant influence on the landing track of the aircraft. It can be concluded that the automatic landing system with LFPIO optimized parameters can successfully guide an aircraft flying through the vertical wind disturbance along the command track.

6. Conclusions

In this paper, we established the automatic carrier landing system in Simulink environment for unmanned aerial vehicle in six-

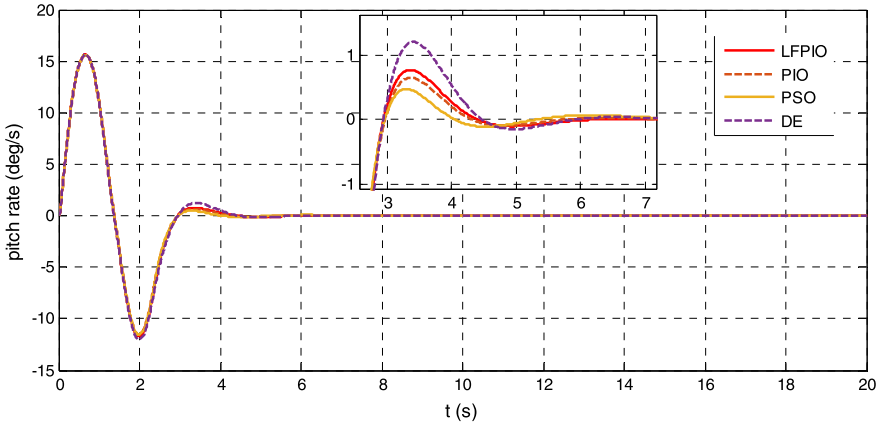

Fig. 14. Comparative results of pitch rate.

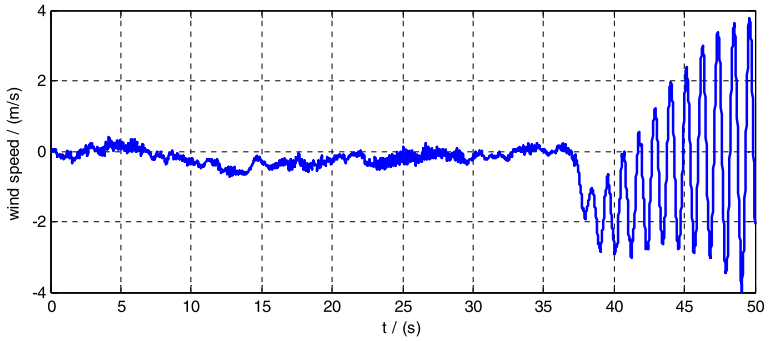

Fig. 15. vertical wind disturbance.

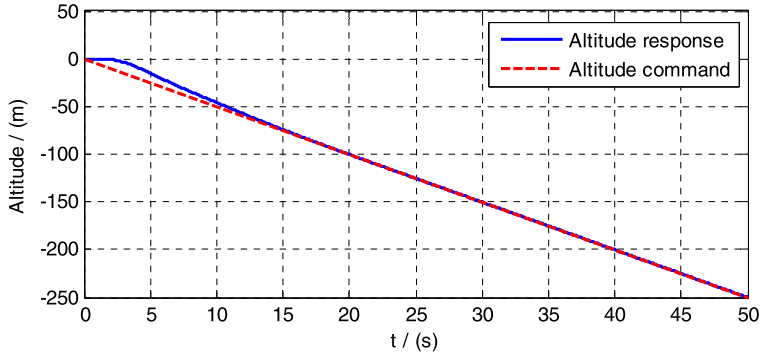

Fig. 16. Altitude response of the aircraft.

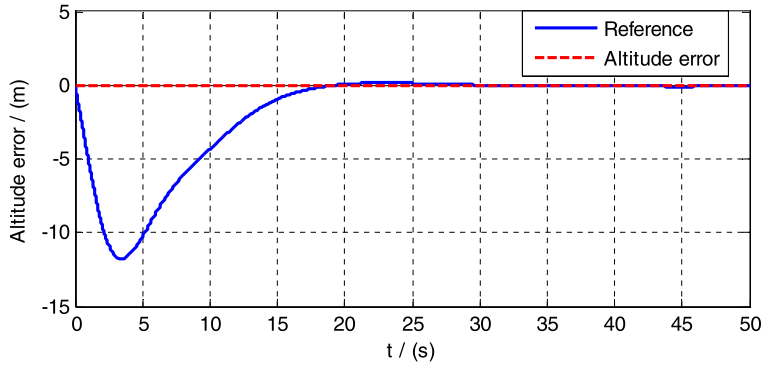

Fig. 17. Altitude error of the aircraft.

degree-of freedom nonlinear model. Then we introduce the basic PIO algorithm and Lévy flight based PIO algorithm and applied the LFPIO to the parameter optimization in ACLS. The comparative experiment of the fitness function value of LFPIO with other algorithms was conducted and LFPIO had better performance in jumping out of the local optimal solution. The optimization results of LFPIO was analyzed and response more steadily and rapidly to the vertical command and the aircraft can successfully accomplish the landing mission through the wind disturbance.

In the future, we will continue our research on the optimization of the control parameter in automatic carrier landing system. In order to embody the requirement of control precision and steady in a better way, we will devote ourselves to the cost function development and do more research on the improvement on the multi objective optimization.

Conflict of interest statement

We have no conflict of interest.

Acknowledgements

This work was partially supported by National Natural Science Foundation of China under grant #61673327, #61425008 and #61333004, and Aeronautical Science Foundation of China under grant #2015ZA51013. The authors would like to thank the editors and reviewers for their critical review of this manuscript.

Appendix A. Supplementary material

Supplementary material related to this article can be found online at http://dx.doi.org/10.1016/j.ast.2016.11.012.

References

[1] J. Urnes, R. Hess, Development of the F/A-18A automatic carrier landing system, J. Guid. Control Dyn. 8 (3) (2015) 289–295.
[2] J. Urnes, R. Moomaw, R. Huff, H-Dot automatic carrier landing system for approach control in turbulence, J. Guid. Control Dyn. 4 (2) (1981) 177–183.
[3] A. Prickett, C. Parkes, Flight testing of the F/A-18E/F automatic carrier landing system, in: Proceedings of IEEE Conference on Aerospace, Big Sky, MT, USA, 10–17 March 2001, IEEE, 2001, pp. 2593–2612.
[4] R. Niewoehner, I. Kaminer, Design of an autoland controller for an F-14 aircraft using H-infinity synthesis, J. Guid. Control Dyn. 19 (3) (1996) 656–663.
[5] M. Subrahmanyam, H-infinity design of F/A-18A automatic carrier landing system, J. Guid. Control Dyn. 17 (1) (1994) 187–191.
[6] M. Dorigo, M. Birattari, Ant colony optimization, IEEE Comput. Intell. Mag. 28 (4) (2010) 28–39.
[7] J. Kennedy, R. Eberhart, Particle swarm optimization, in: Proceedings of IEEE International Conference on Neural Networks, vol. 4, 1995, pp. 1942–1948.
[8] D. Karaboga, B. Basturk, On the performance of artificial bee colony (ABC) algorithm, Appl. Soft Comput. 8 (1) (2008) 687–697.
[9] D. Karaboga, B. Basturk, A powerful and efficient algorithm for numerical function optimization: artificial bee colony (ABC) algorithm, J. Glob. Optim. 39 (3) (2007) 459–471.
[10] R. Storn, K. Price, Differential evolution – a simple and efficient heuristic for global optimization over continuous spaces, J. Glob. Optim. 11 (4) (1997) 341–359.
[11] H. Duan, S. Li, Y. Shi, Predator–prey brain storm optimization for DC brushless motor, IEEE Trans. Magn. 49 (10) (2013) 5336–5340.
[12] Z. Zhan, J. Zhang, Y. Shi, et al., A modified brain storm optimization, in: Proceedings of Evolutionary Computation, 10–15 June, Brisbane, Australia, IEEE, 2012, pp. 1–8.
[13] Y. Shi, J. Xue, Y. Wu, Multi-objective optimization based on brain storm optimization Algorithm, Int. J. Swarm Intell. Res. 4 (3) (2013) 1–21.
[14] J. Li, H. Duan, Simplified brain storm optimization approach to control parameter optimization in F/A-18 automatic carrier landing system, Aerosp. Sci. Technol. 42 (2015) 187–195.
[15] H. Duan, P. Qiao, Pigeon-inspired optimization: a new swarm intelligence optimizer for air robot path planning, Int. J. Intell. Comput. Cybern. 7 (1) (2014) 24–37.
[16] J. Zhao, R. Zhou, Pigeon-inspired optimization applied to constrained gliding trajectories, Nonlinear Dyn. 82 (4) (2015) 1–15.
[17] Y. Deng, H. Duan, Control parameter design for automatic carrier landing system via pigeon-inspired optimization, Nonlinear Dyn. 85 (1) (2016) 1–10.
[18] R. Dou, H. Duan, Pigeon inspired optimization approach to model prediction control for unmanned air vehicles, Aircr. Eng. Aerosp. Technol. 88 (1) (2016) 108–116.
[19] C. Li, H. Duan, Target detection approach for UAVs via improved pigeon-inspired optimization and edge potential function, Aerosp. Sci. Technol. 39 (2014) 352–360.
[20] H. Qiu, H. Duan, Multi-objective pigeon-inspired optimization for brushless direct current motor parameter design, Sci. China, Technol. Sci. 58 (11) (2015) 1915–1923.
[21] L. Gan, H. Duan, Robust binocular pose estimation based on pigeon inspired optimization, in: Proceedings of IEEE 10th Conference on Industrial Electronics and Applications, Auckland, New Zealand, 15–17 June 2015, IEEE, 2015, pp. 1043–1048.
[22] X. Zhang, H. Duan, Pigeon inspired optimization approach to multiple UAVs formation reconfiguration controller design, in: Proceedings of IEEE Chinese Guidance, Navigation and Control Conference, Yantai, China, 8–10 August 2014, IEEE, 2014, pp. 2707–2712.
[23] H. Sun, H. Duan, PID controller design based on prey-predator pigeon-inspired optimization algorithm, in: Proceedings of IEEE International Conference on Mechatronics and Automation, Tianjin, China, 3–6 August, IEEE, 2014, pp. 1416–1421.
[24] G. Viswanathan, V. Afanasyev, S. Buldyrev, et al., Lévy flight search patterns of wandering albatrosses, Nature 381 (6581) (1996) 413–415.
[25] D. Reible, S. Mohanty, A Lévy flight-random walk model for bioturbation, Environ. Toxicol. Chem. 21 (4) (2002) 875–881.
[26] A. Chakraborty, P. Seiler, G. Balas, Susceptibility of F/A-18 flight controllers to the falling-leaf mode: linear analysis, J. Guid. Control Dyn. 34 (1) (2011) 57–72.
[27] M. Napolitano, A. Paris, B. Seanor, et al., Estimation of the longitudinal aerodynamic parameters from flight data for the NASA F/A-18 HARV, in: AIAA Atmospheric Flight Mechanics Conference, San Diego, USA, 29–31 July 1996, AIAA, 1996, pp. 469–478.
[28] M. Napolitano, A. Paris, B. Seanor, et al., Estimation of the lateral-directional aerodynamic parameters from flight data for the NASA F/A-18 HARV, in: AIAA Atmospheric Flight Mechanics Conference, San Diego, USA, AIAA, 29–31 July 1996, 1996, pp. 479–489.
[29] S. Balsamo, A. Marin, Separable solutions for Markov processes in random environments, Eur. J. Oper. Res. 229 (2) (2013) 391–403.
[30] R. Mantegna Fast, accurate algorithm for numerical simulation of Lévy stable stochastic processes, Phys. Rev. E 49 (5) (1994) 4677–4683.